Letter

Flat bands with band crossings enforced by symmetry representation

Yoonseok Hwang,[1,2,3] Jun-Won Rhim,[1,2,4] and Bohm-Jung Yang[1,2,3,*]

[1]*Center for Correlated Electron Systems, Institute for Basic Science (IBS), Seoul 08826, Korea*
[2]*Department of Physics and Astronomy, Seoul National University, Seoul 08826, Korea*
[3]*Center for Theoretical Physics (CTP), Seoul National University, Seoul 08826, Korea*
[4]*Department of Physics, Ajou University, Suwon 16499, Korea*

(Received 3 June 2021; accepted 27 July 2021; published 5 August 2021)

Flat bands have band crossing points with other dispersive bands in many systems including the canonical flat-band models in the Lieb and kagome lattices. Here we show that some of such band degeneracy points of nondegenerate flat bands are unavoidable because of the symmetry representation (SR) of flat bands under unitary symmetry. We refer to such a band degeneracy point of flat bands as a *SR-enforced band crossing*. SR-enforced band crossing is distinct from the conventional band degeneracy protected by symmetry eigenvalues or topological charges in that its protection requires both specific symmetry representation and band flatness of the flat band, simultaneously. Even n-fold rotation C_n ($n = 2, 3, 4, 6$) symmetry, which cannot protect band degeneracy without additional symmetries due to its abelian nature, can protect SR-enforced band crossings in flat-band systems. In two-dimensional flat-band systems with C_n symmetry, when the degeneracy of a SR-enforced band crossing is lifted by a C_n *symmetry-preserving perturbation*, we obtain a nearly flat Chern band. Our theory not only explains the origin of the band crossing points of FBs existing in various models, but also gives a strict no-go theorem for isolated FBs in a given lattice arising from the SR.

DOI: 10.1103/PhysRevB.104.L081104

Introduction. Flat bands (FBs) [1–23] have been considered an ideal playground to study strong correlation physics because of the dispersionless energy-band structure. However, recent studies of twisted bilayer graphene [24–26] and kagome materials [27–29] have shown that not only the flat energy dispersion itself but also the characteristics of FB wave functions are important to understand fundamental properties of FB systems. For example, the FBs in kagome materials are promising candidates to observe nearly flat Chern bands with nontrivial topology [30–32]. Also, the FB of twisted bilayer graphene at magic angle has demonstrated the first material realization of fragile band topology [33–35].

In many systems, FBs often accompany band crossing points with other dispersive bands [36–39]. Representative examples include the FB in the kagome lattice with a quadratic band crossing at the Brillouin zone (BZ) center, and that in the Lieb lattice with triple degeneracy at a BZ corner. A FB with a band crossing is called a singular FB (SFB) [38,39] when the relevant momentum-space eigenstate has zeros. Because of the inherent interband coupling, SFBs exhibit nontrivial geometric responses. For instance, it was recently shown that a SFB with a quadratic band crossing exhibits anomalous Landau level spreading whose energy width measures the quantum distance of its momentum-space eigenstate [39–41].

In this Letter, we show that there is a class of FBs with unavoidable band crossings arising from the symmetry representation and band flatness of FBs, focusing on nondegenerate FBs. To demonstrate this, we systematically investigate the symmetry representation (SR) of a compact localized state (CLS) under unitary symmetry. A CLS is a real-space localized eigenstate of the FB, which is confined within a finite region [42–50]. We examine the SR of the CLS by considering it as a hybrid molecular state of atomic orbitals in a given lattice, and show that irremovable singular points appear when there is a mismatch in the SRs between the CLS and its constituent atomic orbitals at high-symmetry points. We refer to such a band crossing of FBs enforced by the SR of the CLS as a *SR-enforced band crossing*.

SR-enforced band crossing is distinct from the conventional band degeneracy protected by symmetry eigenvalues or topological charges in that its protection requires both specific SR and band flatness of the FB, simultaneously. For instance, even n-fold rotation C_n ($n = 2, 3, 4, 6$) symmetry, which cannot protect band degeneracy without additional symmetries as it has only one-dimensional irreducible representations (IRs), can protect SR-enforced band crossings in FB systems. When the atomic orbitals constituting the CLS are located at maximal Wyckoff positions, the existence of the SR-enforced band crossing can be determined via a determinant test we developed. On the other hand, if the constituent atomic orbitals are located at generic Wyckoff positions, the constraints from multiple symmetries can also give SR-enforced band crossings, which is applicable to various line and split graphs [37,51–54].

Interestingly, in two-dimensional lattices with C_n rotation symmetry ($n = 2, 3, 4, 6$), a nearly FB with nonzero Chern number must emerge when the degeneracy of a single SR-enforced band crossing is lifted. This clearly shows that

*bjyang@snu.ac.kr

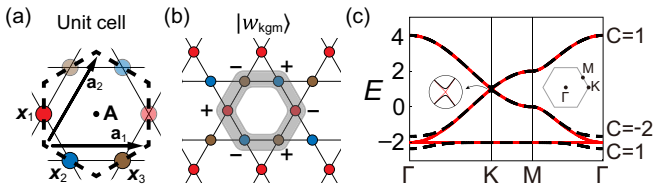

FIG. 1. Kagome lattice. (a) The unit cell composed of three sublattices located at $\boldsymbol{x}_1 = -\frac{1}{2}\boldsymbol{a}_1$, $\boldsymbol{x}_2 = -\frac{1}{2}\boldsymbol{a}_2$, and $\boldsymbol{x}_3 = \frac{1}{2}\boldsymbol{a}_1 - \frac{1}{2}\boldsymbol{a}_2$, respectively, where $\boldsymbol{a}_1 = (1, 0)$ and $\boldsymbol{a}_2 = (\frac{1}{2}, \frac{\sqrt{3}}{2})$ are primitive lattice vectors. The Wyckoff position $\boldsymbol{A}$ corresponds to the unit-cell center. (b) The CLS $|w_{\rm kgm}(\boldsymbol{R})\rangle$ whose shape is depicted by the gray region. The sign ($\pm$) near each site denotes the amplitude $S_\alpha(\boldsymbol{R}')$ of the CLS. (c) The band structure (red solid lines) of $H_{\rm kgm}(\boldsymbol{k})$ having a FB with two-fold degeneracy at Γ. The black dashed lines correspond to the case with additional C_6-preserving perturbation $\delta H_{\rm kgm}(\boldsymbol{k})$. C near each gapped band denotes its Chern number.

the FB with SR-enforced band crossing is a promising platform to achieve nearly flat Chern bands [30–32,55–60].

Kagome lattice. We illustrate the general idea of SR-enforced band crossing by considering the FB in the kagome lattice composed of three sublattices as shown in Fig. 1. We place an s orbital at each sublattice. The kagome lattice belongs to the wallpaper group *p6mm* generated by a six-fold rotation C_6 and two mirrors M_x and M_y that flip the sign of the x and y coordinates, respectively. Below we focus on the role of C_6 symmetry on the band crossing of the FB. The tight-binding Hamiltonian including only the nearest-neighbor hopping with the unit amplitude is

$$H_{\rm kgm}(\boldsymbol{k}) = \begin{pmatrix} 0 & 1+Q_1\overline{Q_2} & Q_1+Q_1\overline{Q_2} \\ c.c. & 0 & 1+Q_1 \\ c.c. & c.c. & 0 \end{pmatrix}, \quad (1)$$

where $Q_i = e^{-i\boldsymbol{k}\cdot\boldsymbol{a}_i}$ with lattice vectors $\boldsymbol{a}_i$ $(i = 1, 2)$, and $\overline{x}$ denotes the complex conjugation ($c.c.$) of x (see the Supplemental Material (SM) [61]). The band structure of $H_{\rm kgm}(\boldsymbol{k})$ exhibits a FB at the energy -2 with a band crossing at the momentum $\Gamma = (0, 0)$ as shown in Fig. 1(c). Conventionally, the degeneracy can be understood in terms of two-dimensional IRs of C_3 symmetry combined with time-reversal T or a mirror symmetry. However, we find that the degeneracy survives even when all symmetries except C_6 are broken as long as the band flatness is maintained. Degeneracy protection by an abelian symmetry is a hallmark of SR-enforced band crossing of FBs.

For any FB model with finite-ranged hoppings, an eigenstate of FB $|\hat{u}(\boldsymbol{k})\rangle$ can always be expressed as Laurent polynomials in Q_i [38,46]. A relevant CLS is defined by a Fourier transform of $|\hat{u}(\boldsymbol{k})\rangle$ [61]. We refer to $|\hat{u}(\boldsymbol{k})\rangle$ as a Fourier transform of CLS (FT-CLS). In general, the center of a CLS is confined within a unit cell. For a unit cell located at $\boldsymbol{R}$, the relevant CLS is expressed as $|w(\boldsymbol{R})\rangle = \sum_{\boldsymbol{R}',\alpha} S_\alpha(\boldsymbol{R}')|\boldsymbol{R}+\boldsymbol{R}', \alpha\rangle$ where $\boldsymbol{R}$ and $\boldsymbol{R}'$ are lattice vectors, α is an orbital index, and $|\boldsymbol{R}, \alpha\rangle$ denotes an electron located at $\boldsymbol{R} + \boldsymbol{x}_\alpha$ $(\alpha = 1, \ldots, n_{\rm tot})$ where $n_{\rm tot}$ indicates the total number of orbitals per unit cell. $S_\alpha(\boldsymbol{R}')$ is nonzero only inside a finite region, referred to as a *shape* here. Note that we always require that there is no common divisor polynomial for all elements of $|\hat{u}(\boldsymbol{k})\rangle$, which means that a CLS is *elementary*, not expressed as a sum of other CLSs. For $H_{\rm kgm}(\boldsymbol{k})$, FT-CLS and CLS are given by $|\hat{u}_{\rm kgm}(\boldsymbol{k})\rangle = (1 - Q_1, Q_2 - 1, 1 - \overline{Q_1}Q_2)$ and $|w_{\rm kgm}(\boldsymbol{R})\rangle = |\boldsymbol{R}, 1\rangle - |\boldsymbol{R}+\boldsymbol{a}_1, 1\rangle + |\boldsymbol{R}+\boldsymbol{a}_2, 2\rangle - |\boldsymbol{R}, 2\rangle + |\boldsymbol{R}, 3\rangle - |\boldsymbol{R}-\boldsymbol{a}_1+\boldsymbol{a}_2, 3\rangle$, respectively. The shape of $|w_{\rm kgm}(\boldsymbol{R})\rangle$ is illustrated in Fig. 1(b).

Importantly, $|\hat{u}_{\rm kgm}(\boldsymbol{k})\rangle$ has a zero at Γ, i.e., $|\hat{u}_{\rm kgm}(\Gamma)\rangle = 0$. In general, when $|\hat{u}(\boldsymbol{k})\rangle$ becomes zero at a momentum, the corresponding FB and its zero are called a singular FB (SFB) and a singular point, respectively. A SFB must have a band crossing with other dispersive bands at the singular point [38]. A rigorous proof of the relation between zeros of FT-CLS and band crossing points is shown in SM [61]. (Note that the number of degenerate states at the singular points depends on the symmetry of the model.) Hence, the singularity of $|\hat{u}_{\rm kgm}(\boldsymbol{k})\rangle$ indicates the existence of band crossing points of FB in $H_{\rm kgm}(\boldsymbol{k})$. Below we further show that the singularity originates from the SR of the CLS.

Symmetry representation of CLS. Now we discuss the symmetry property of CLS. The hexagonal CLS $|w_{\rm kgm}(\boldsymbol{R})\rangle$ can be considered as a hybrid orbital formed by six atomic orbitals. Interestingly, a hybrid orbital can have symmetry that its constituent atomic orbitals cannot have. For instance, while each atomic orbital does not have C_6, the CLS $|w_{\rm kgm}(\boldsymbol{R})\rangle$ is symmetric under C_6. Specifically, $|w_{\rm kgm}(\boldsymbol{R})\rangle$ is centered at the Wyckoff position $\boldsymbol{A} = (0, 0)$ and has a C_6 eigenvalue $\xi_3 = -1$ where $\xi_l = e^{i\pi l/3}$ $(l = 0, \ldots, 5)$, as readily inferred from its shape. The center $\boldsymbol{A}$ and symmetry eigenvalue ξ_3 define the SR $\boldsymbol{A}_3$ of the CLS $|w_{\rm kgm}(\boldsymbol{R})\rangle$.

According to the SR, the CLS and FT-CLS transform under C_6 as

$$\hat{C}_6|w_{\rm kgm}(\boldsymbol{R})\rangle = |w_{\rm kgm}(O_{C_6}\boldsymbol{R})\rangle\,\xi_3, \quad (2)$$

$$U_{C_6}(\boldsymbol{k})|\hat{u}_{\rm kgm}(\boldsymbol{k})\rangle = |\hat{u}_{\rm kgm}(O_{C_6}\boldsymbol{k})\rangle\,\xi_3, \quad (3)$$

where O_{C_6} and $U_{C_6}(\boldsymbol{k})$ indicate the matrix representations of C_6 in real and orbital spaces, respectively [61]. A CLS with its center at $\boldsymbol{A}$ and C_6 eigenvalue ξ_3, generally denoted as $\boldsymbol{A}_3$-CLS, follows the same symmetry transformation in Eqs. (2) and (3).

SR-enforced band crossing. Remarkably, the band crossing in $H_{\rm kgm}(\boldsymbol{k})$ is enforced by $\boldsymbol{A}_3$ SR of the CLS. To elucidate this, let us consider C_6 eigenvalues at Γ, a unique C_6-invariant momentum. $\boldsymbol{A}_3$-CLS always occupies all three sublattices. At Γ point in the BZ, the orbitals at these sublattices induce three IRs with C_6 eigenvalues 1, $e^{2\pi i/3}$ and $e^{-2\pi i/3}$, respectively. On the other hand, according to Eq. (3), C_6 eigenvalue of the FT-CLS $|\hat{u}_{\rm kgm}(\boldsymbol{k})\rangle$ is -1, if the FT-CLS is nonsingular at Γ, i.e., $|\hat{u}_{\rm kgm}(\Gamma)\rangle \neq 0$. We refer to such a symmetry eigenvalue of FT-CLS under the assumption of nonsingularity as a *superficial* symmetry eigenvalue. Clearly, the superficial C_6 eigenvalue of FT-CLS does not match any C_6 eigenvalue of the IRs induced from its constituent atomic orbitals: $-1 \notin \{1, e^{2\pi i/3}, e^{-2\pi i/3}\}$. The only way to circumvent this contradiction is that $|\hat{u}_{\rm kgm}(\Gamma)\rangle$ is singular, i.e., $|\hat{u}_{\rm kgm}(\Gamma)\rangle = 0$. Hence, a FB corresponding to $\boldsymbol{A}_3$-CLS cannot exist as a gapped isolated band, and it must have a SR-enforced band crossing at Γ. We note that this *no-go* statement for gapped FB with $\boldsymbol{A}_3$ SR holds for *any* FB model defined in the kagome lattice and any CLS with $\boldsymbol{A}_{1,3,5}$ SRs.

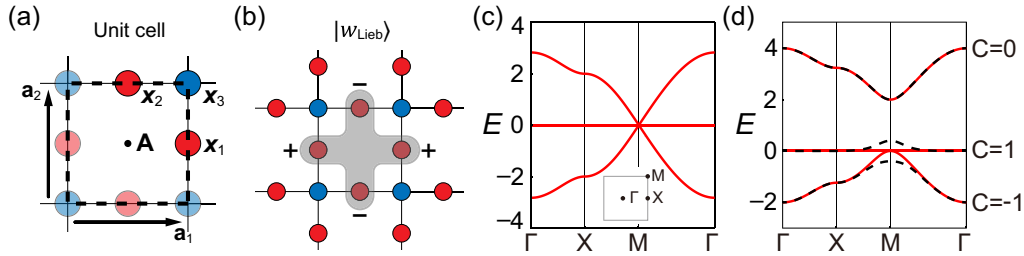

FIG. 2. Lieb lattice. (a) The unit cell composed of three sublattices at $\boldsymbol{x}_{1,2,3}$. (b) The CLS $|w_{\rm Lieb}(\boldsymbol{R})\rangle$ composed of orbitals located at the sublattices $\boldsymbol{x}_1$ and $\boldsymbol{x}_2$. (c) Band structure of $H^{(0)}_{\rm Lieb}(\boldsymbol{k})$ with a three-fold degeneracy at M. (d) Band structure of $H_{\rm Lieb}(\boldsymbol{k})$ with on-site potential $\epsilon_3 = 2.0$ at the sublattice 3 (red lines). There is a two-fold degeneracy at M. Black dashed lines indicate bands when a C_4-preserving perturbation $\delta H_{\rm Lieb}(\boldsymbol{k})$ is added. C near each band denotes the corresponding Chern number.

We further search SR-enforced band crossing at K and M in the BZ, which correspond to C_3 and C_2 invariant momenta, respectively. The FB corresponding to $\boldsymbol{A}_3$-CLS has superficial C_3 (C_2) eigenvalue 1 (-1) at K (M). On the other hand, the IRs induced from constituent atomic orbitals have C_3 (C_2) eigenvalues 1, $e^{2\pi i/3}$ and $e^{-2\pi i/3}$ (-1, -1, and 1). Hence, the mismatch of symmetry eigenvalues does not happen, and there is no SR-enforced band crossing at K and M.

Determinant criterion for SR-enforced band crossing. Based on the above discussion, we now propose a general condition for SR-enforced band crossings. At Γ, Eq. (3) is reduced to $\mathcal{P}(\Gamma)|\hat{u}(\Gamma)\rangle = 0$ where $\mathcal{P}(\Gamma) = U_{C_6}(\Gamma) - \xi_3 \mathbb{1}_3$ and $\mathbb{1}_3$ is the 3×3 identity matrix. A condition for having SR-enforced band crossing is encapsulated in $\mathrm{Det}\mathcal{P}(\Gamma) \neq 0$. This ensures a singular FT-CLS, i.e., $|\hat{u}(\Gamma)\rangle = 0$. Since C_6 eigenvalues of the atomic orbitals constituting CLS are equivalent to eigenvalues of $U_{C_6}(\Gamma)$, the condition $\mathrm{Det}\mathcal{P}(\Gamma) \neq 0$ implies that the superficial C_6 eigenvalue ξ_3 of FT-CLS does not match any of those of the constituent atomic orbitals.

In the kagome lattice, all atomic orbitals contribute to the hybrid orbital of the CLS. However, in general, a CLS can also occupy only a part of atomic orbitals as in the Lieb lattice model discussed below. We denote a set of such atomic orbitals unoccupied by CLS as $\{\alpha_\varnothing\}$. Then a general condition for SR-enforced band crossing related to unitary symmetry σ is as follows. When a given SR under σ constrains FT-CLS such that $\mathcal{P}(\bar{\boldsymbol{k}}_\sigma)|\hat{u}(\bar{\boldsymbol{k}}_\sigma)\rangle = 0$ at a high-symmetry point $\bar{\boldsymbol{k}}_\sigma$ for σ,

$$\mathrm{Det}_{\{\alpha_\varnothing\}}\mathcal{P}(\bar{\boldsymbol{k}}_\sigma) \neq 0 \tag{4}$$

indicates a SR-enforced band crossing at $\bar{\boldsymbol{k}}_\sigma$. The detailed expression of $\mathcal{P}(\bar{\boldsymbol{k}}_\sigma)$ is determined by unitary symmetry σ and SR of a given CLS [61], and $\mathrm{Det}_{\{\alpha_\varnothing\}}\mathcal{O}$ is the determinant of $\mathcal{O}$ after removing the rows and columns corresponding to the orbital indices $\{\alpha_\varnothing\}$.

When only a single unitary symmetry is concerned, Eq. (4) is the most general condition for SR-enforced band crossing. However, when the constituent atomic orbitals are located at nonmaximal Wyckoff positions, they can support all possible symmetry eigenvalues including the superficial eigenvalue of FT-CLS, thus mismatch of symmetry eigenvalues does not occur. Even in such cases, nevertheless, SR-enforced band crossing can occur when two or more symmetries are considered. Suppose a SR of CLS under multiple symmetries imposes N conditions on the FT-CLS: $\mathcal{P}_I(\bar{\boldsymbol{k}})|\hat{u}(\bar{\boldsymbol{k}})\rangle = 0$ ($I = 1, \ldots, N$). When the constituent atomic orbitals of the CLS cannot span the FT-CLS at a high-symmetry point $\bar{\boldsymbol{k}}$, these N conditions lead to $|\hat{u}(\bar{\boldsymbol{k}})\rangle = 0$, hence the band crossing point at $\bar{\boldsymbol{k}}$. We illustrate this idea using the line graph of the Lieb lattice below.

Lieb lattice. FB with band crossing enforced by SR for C_4 exists in the Lieb lattice composed of three sublattices, which belongs to the wallpaper group $p4mm$ (see Fig. 2). A tight-binding model $H_{\rm Lieb}(\boldsymbol{k})$ with nearest-neighbor hopping exhibits a FB having a three-fold degeneracy at the momentum $M = (\pi, \pi)$ [see Fig. 2(b)]. The relevant CLS $|w_{\rm Lieb}(\boldsymbol{R})\rangle$ is centered at the Wyckoff position $\boldsymbol{A} = (0, 0)$ and has a C_4 eigenvalue -1. It is worth noting that the atomic orbitals constituting the CLS $|w_{\rm Lieb}(\boldsymbol{R})\rangle$ occupy only the sublattice 1 and 2, i.e., $\{\alpha_\varnothing\} = \{3\}$. Therefore, the constituent atomic orbitals form IRs with C_4 eigenvalues $\pm i$ at M, while the FB has a superficial C_4 eigenvalue -1 at M. This mismatch of C_4 eigenvalue at M indicates a singular FT-CLS, i.e., $|\hat{u}_{\rm Lieb}(M)\rangle = 0$, and a SR-enforced band crossing at M. The same result can also be obtained by the determinant criterion in Eq. (4), which becomes $\mathrm{Det}_{\{3\}}\mathcal{P}(M) = 2$ where $\mathcal{P}(M) = U_{C_4}(M) + \mathbb{1}_3$. The determinant criterion for C_2 SR-enforced band crossing applied at $\bar{\boldsymbol{k}} = \Gamma, X, Y, M$ also predicts a SR-enforced band crossing only at M.

It is worth noting that the fact that $|w_{\rm Lieb}(\boldsymbol{R})\rangle$ does not occupy the sublattice 3 is critical for the presence of the band crossing at M. For example, one can consider another CLS with its center at $\boldsymbol{A}$ and C_4 eigenvalue -1 whose constituent atomic orbitals occupy all three sublattices. In this case, the corresponding FB is not enforced to have a band crossing point, hence it can be gapped [61].

Dice lattice. FB with band crossings enforced by SR for C_3 exists in the dice lattice composed of three sublattices, which belongs to the wallpaper group $p6mm$ (see Fig. 3). Considering only nearest-neighbor hoppings, a tight-binding model $H_{\rm dice}(\boldsymbol{k})$ exhibits a FB with three-fold degeneracy at K and $-K$, respectively, as shown in Fig. 3(c). The CLS of the FB $|w_{\rm dice}(\boldsymbol{R})\rangle$ is composed of the atomic orbitals located at the sublattice 2 and 3, as shown in Fig. 3(b), thus $\{\alpha_\varnothing\} = \{1\}$. Also, it is centered at $\boldsymbol{A} = (0, 0)$ and has C_3 eigenvalue 1. Then the determinant criterion, $\mathrm{Det}_{\{1\}}[U_{C_3}(\pm K) - \mathbb{1}_3] = 3$, indicates SR-enforced band crossings at $\pm K$.

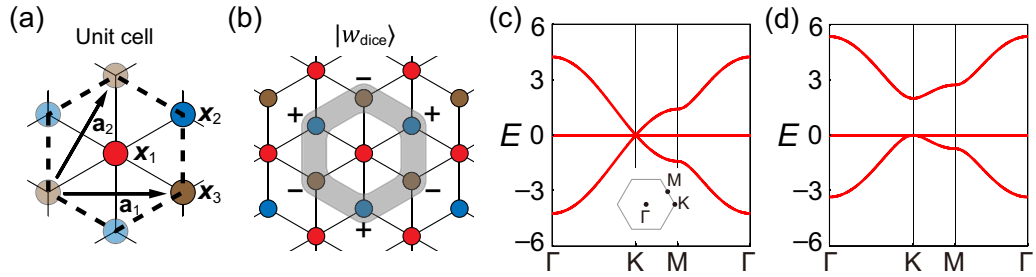

FIG. 3. Dice lattice. (a) The unit cell composed of three sublattices. (b) The CLS $|w_{\rm dice}(\boldsymbol{R})\rangle$ composed of orbitals located at the sublattices $\boldsymbol{x}_2$ and $\boldsymbol{x}_3$. (c) Band structure of $H_{\rm dice}(\boldsymbol{k})$ with a three-fold degeneracy at K. (d) Band structure of $H_{\rm dice}(\boldsymbol{k})$ with on-site potential $\epsilon_1 = 2.0$ at the sublattice 1. There are two-fold degeneracies at $\pm K$.

FBs in lattices with two orthogonal mirrors. When the atomic orbitals are located at generic Wyckoff positions, the determinant criterion in Eq. (4) does not work. Even in this case, however, SR-enforced band crossings can appear because of multiple symmetries. As a representative example, we consider a square lattice with four sublattices shown in Fig. 4(a), belonging to the wallpaper group *p4mm* as the Lieb lattice. Here, we focus on two mirror symmetries M_x and M_y. When the hopping structure takes a particular configuration shown in Fig. 4(a), the lattice is called a line graph [15,37,54] of the Lieb lattice. The relevant tight-binding Hamiltonian is denoted as $H_{\rm LG}(\boldsymbol{k})$ whose band structure possesses two FBs at the energy $E = 0$ and 2, respectively [see Fig. 4(c)]. The FB with $E = 0$ (2) has a band crossing point at Γ (M) and the corresponding CLS $|w_{--}(\boldsymbol{R})\rangle$ ($|w_{++}(\boldsymbol{R})\rangle$) is shown in Fig. 4(b). Note that the lower indices of CLSs denote the eigenvalues of M_x and M_y in order.

Now let us consider the SR of $|w_{++}(\boldsymbol{R})\rangle$ under mirror symmetries. Because of its SR, the FT-CLS $|\hat{u}_{++}(\boldsymbol{k})\rangle$ satisfies $U_{M_{x,y}}(M)|\hat{u}_{++}(M)\rangle = |\hat{u}_{++}(M)\rangle$ where 4×4 matrices $U_{M_x}(M)$ and $U_{M_y}(M)$ are given by the direct sum $(-\tau_0)\oplus\tau_1$ and $\tau_1\oplus(-\tau_0)$ in terms of the Pauli matrices $\tau_{0,1,2,3}$. These two conditions necessarily lead to a singular FT-CLS satisfying $|\hat{u}_{++}(M)\rangle = 0$. This shows that a FB corresponding to the same SR as $|w_{++}(\boldsymbol{R})\rangle$ cannot be gapped in any model with arbitrary hopping structure including the line graph configuration. Similarly, it can also be shown that the SR of $|w_{--}(\boldsymbol{R})\rangle$ leads to the singular FT-CLS at Γ. It is worth noting that although two orthogonal commuting mirrors allow only one-dimensional IRs, they can induce SR-enforced band crossing of FBs.

Nearly flat Chern bands. What happens if the degeneracy of SR-enforced band crossing is lifted? When a single band crossing with two-fold degeneracy is enforced by SR under C_n symmetry alone and the degeneracy is lifted by a C_n-preserving perturbation, the resulting gapped nearly FB carries a nonzero Chern number. This is because the C_n eigenvalue of the nearly FB at the momentum where the degeneracy is lifted is different from the superficial C_n eigenvalue of the FB so that the gapped FB is not band representable, thus topologically nontrivial [62].

In the case of $H_{\rm kgm}(\boldsymbol{k})$, a FB has a single SR-enforced band crossing at Γ. Hence, the FB becomes a nearly flat Chern band when a C_6-preserving perturbation $\delta H_{\rm kgm}(\boldsymbol{k})$, which lifts the degeneracy at Γ, is added [see Fig. 1(c)]. The nearly flat Chern band induced by spin-orbit coupling can be understood in this way [27,30,63]. The same mechanism can also be applied to magnon bands in the kagome ferromagnet [64–66].

In the case of $H_{\rm Lieb}(\boldsymbol{k})$, the FB has a three-fold degeneracy at M, which can be split into two-fold and nondegenerate ones, by introducing on-site potential ϵ_3 at the sublattice 3. Crucially, this procedure does not break the flat dispersion of FB because the CLS $|w_{\rm Lieb}(\boldsymbol{R})\rangle$ does not occupy the sublattice 3. The SR-enforced degeneracy can be lifted and the FB becomes a nearly flat Chern band as shown in Fig. 2(d), by introducing a perturbation $\delta H_{\rm Lieb}(\boldsymbol{k})$ that preserves C_4 but breaks other symmetries.

Finally, we note that a FB with multiple SR-enforced band crossing points, as in the model $H_{\rm dice}(\boldsymbol{k})$ [Figs. 3(c) and 3(d)], is unnecessary to be a nearly flat Chern band, when the degeneracy is lifted by symmetry-preserving perturbation,

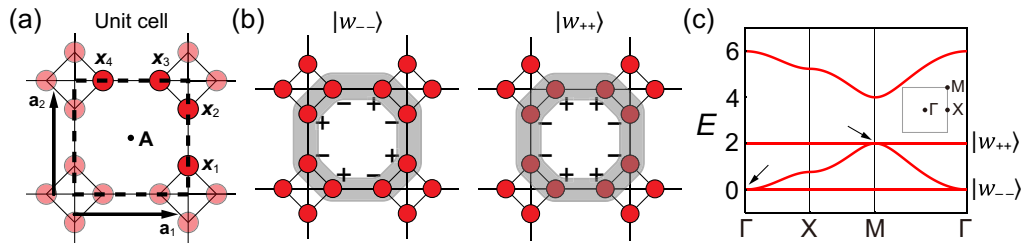

FIG. 4. Line graph of the Lieb lattice. (a) The unit cell composed of four sublattices located at $\boldsymbol{x}_1 = (1/2, -1/4)$ $\boldsymbol{x}_2 = (1/2, 1/4)$, $\boldsymbol{x}_3 = (1/4, 1/2)$ and $\boldsymbol{x}_4 = (-1/4, 1/2)$, respectively. The hoppings between the sites connected by black lines are considered. (b) The CLSs $|w_{++}(\boldsymbol{R})\rangle$ and $|w_{--}(\boldsymbol{R})\rangle$ of $H_{\rm LG}(\boldsymbol{k})$. The lower indices denote M_x and M_y eigenvalues, respectively. (c) Band structure of $H_{\rm LG}(\boldsymbol{k})$. The FB with $E = 0$ ($E = 2$), which corresponds to $|w_{--}(\boldsymbol{R})\rangle$ ($|w_{++}(\boldsymbol{R})\rangle$), has a band crossing point at Γ (M).

as the Berry curvature from different crossing points can be canceled.

Discussion. We have shown that some FBs have unavoidable band crossings with dispersive bands, when there is a SR mismatch between the CLS and its constituent atomic orbitals under unitary symmetry. This result can be applied to any lattices with arbitrary unitary symmetry representations of orbitals. Especially, the notion of SR-enforced band crossing not only explains the origin of the band crossing points of FBs appearing in various lattice models, but also gives a stringent no-go theorem such that a class of FB can never be realized as an isolated FB in a given lattice due to the SR.

We also have shown that lifting the degeneracy of SR-enforced band crossing by symmetry-preserving perturbation gives nearly flat Chern bands. Even the early models of the nearly flat Chern band [31,32] can be adiabatically deformed to FB models with SR-enforced band crossing as shown in SM [61].

We expect that anti-unitary symmetries can provide more examples of FBs with unavoidable band crossings enforced by SR. Further extending the notion of wave function singularity and SR of CLS to degenerate FBs is also an important topic for future research.

Finally, we anticipate that SR of CLS plays an important role in realizing symmetry-protected topological (SPT) phases. In Ref. [67], interacting SPT phases with spinful bosons are obtained from FB models, when many-body ground state, given by a product of CLSs with specific SR, transforms nontrivially under point group symmetries.

Acknowledgments. We thank Sungjoon Park and Sunje Kim for useful discussion. Y.H. and B.-J.Y. were supported by the Institute for Basic Science in Korea (Grant No. IBS-R009-D1), Samsung Science and Technology Foundation under Project No. SSTF-BA2002-06, the National Research Foundation of Korea (NRF) Grant funded by the Korea government (MSIT) (No. 2021R1A2C4002773, and No. NRF-2021R1A5A1032996). J.W.R. was supported by IBS-R009-D1, the National Research Foundation of Korea (NRF) Grant funded by the Korea government (MSIT) (Grant No. 2021R1A2C1010572), and the New Faculty Research Fund of Ajou University.

[1] E. H. Lieb, Two Theorems on the Hubbard Model, Phys. Rev. Lett. **62**, 1201 (1989).
[2] H. Aoki, M. Ando, and H. Matsumura, Hofstadter butterflies for flat bands, Phys. Rev. B **54**, R17296 (1996).
[3] S. D. Huber and E. Altman, Bose condensation in flat bands, Phys. Rev. B **82**, 184502 (2010).
[4] C. Weeks and M. Franz, Flat bands with nontrivial topology in three dimensions, Phys. Rev. B **85**, 041104(R) (2012).
[5] S. Peotta and P. Törmä, Superfluidity in topologically nontrivial flat bands, Nat. Commun. **6**, 8944 (2015).
[6] A. Julku, S. Peotta, T. I. Vanhala, D.-H. Kim, and P. Törmä, Geometric Origin of Superfluidity in the Lieb-Lattice Flat Band, Phys. Rev. Lett. **117**, 045303 (2016).
[7] A. Ramachandran, A. Andreanov, and S. Flach, Chiral flat bands: Existence, engineering, and stability Phys. Rev. B **96**, 161104(R) (2017).
[8] T. Misumi and H. Aoki, New class of flat-band models on tetragonal and hexagonal lattices: Gapped versus crossing flat bands, Phys. Rev. B **96**, 155137 (2017).
[9] B. Pal and K. Saha, Flat bands in fractal-like geometry, Phys. Rev. B **97**, 195101 (2018).
[10] T. Bilitewski and R. Moessner, Disordered flat bands on the kagome lattice, Phys. Rev. B **98**, 235109 (2018).
[11] T. Mizoguchi and M. Udagawa, Flat-band engineering in tight-binding models: Beyond the nearest-neighbor hopping, Phys. Rev. B **99**, 235118 (2019).
[12] T. Mizoguchi and Y. Hatsugai, Molecular-orbital representation of generic flat-band models, Europhys. Lett. **127**, 47001 (2019).
[13] T. Mizoguchi and Y. Hatsugai, Systematic construction of topological flat-band models by molecular-orbital representation, Phys. Rev. B **101**, 235125 (2020).
[14] T. Mizoguchi and Y. Hatsugai, Type-III Dirac cones from degenerate directionally flat bands: Viewpoint from molecular-orbital representation, J. Phys. Soc. Jpn. **89**, 103704 (2020).
[15] C.S. Chiu, Da-Shuai Ma, Zhi-Da Song, B.A. Bernevig, and A.A. Houck, Fragile topology in line-graph lattices with two, three, or four gapped flat bands, Phys. Rev. Research **2**, 043414 (2020).
[16] Y. Hwang, J.-W. Rhim, and B.-J. Yang, Geometric characterization of anomalous Landau levels of isolated flat bands, arXiv:2012.15132.
[17] Y. Kuno, T. Mizoguchi, and Y. Hatsugai, Flat band quantum scar, Phys. Rev. B **102**, 241115(R) (2020).
[18] F. Xie, Z. Song, B. Lian, and B.A. Bernevig, Topology-Bounded Superfluid Weight in Twisted Bilayer Graphene, Phys. Rev. Lett. **124**, 167002 (2020).
[19] Yu-Ping Lin, Chiral flat band superconductivity from symmetry-protected three-band crossings, Phys. Rev. Research **2**, 043209 (2020).
[20] M. Kheirkhah, Y. Nagai, C. Chen, and F. Marsiglio, Majorana corner flat bands in two-dimensional second-order topological superconductors, Phys. Rev. B **101**, 104502 (2020).
[21] C.V. Morfonios, M. Röntgen, M. Pyzh, and P. Schmelcher, Flat bands by latent symmetry, Phys. Rev. B **104**, 035105 (2021).
[22] V. Peri, Zhi-Da Song, B.A. Bernevig, and S.D. Huber, Fragile Topology and Flat-Band Superconductivity in the Strong-Coupling Regime, Phys. Rev. Lett. **126**, 027002 (2021).
[23] W. Maimaiti, A. Andreanov, and S. Flach, Flat-band generator in two dimensions, Phys. Rev. B **103**, 165116 (2021).
[24] R. Bistritzer and A. H. MacDonald, Moiré bands in twisted double-layer graphene, Proc. Natl. Acad. Sci. USA **108**, 12233 (2011).
[25] Y. Cao, V. Fatemi, A. Demir, S. Fang, S. L. Tomarken, J. Y. Luo, J. D. Sanchez-Yamagishi, K. Watanabe, T. Taniguchi, E. Kaxiras *et al.*, Correlated insulator behaviour at half-filling in magic-angle graphene superlattices, Nature (London) **556**, 80 (2018).
[26] Y. Cao, V. Fatemi, S. Fang, K. Watanabe, T. Taniguchi, E. Kaxiras, and P. Jarillo-Herrero, Unconventional superconduc-

tivity in magic-angle graphene superlattices, Nature (London) **556**, 43 (2018).

[27] L. Ye, M. Kang, J. Liu, F. Von Cube, C. R. Wicker, T. Suzuki, C. Jozwiak, A. Bostwick, E. Rotenberg, D. C. Bell *et al.*, Massive Dirac fermions in a ferromagnetic kagome metal, Nature (London) **555**, 638 (2018).

[28] Z. Li, J. Zhuang, L. Wang, H. Feng, Q. Gao, X. Xu, W. Hao, X. Wang, C. Zhang, K. Wu *et al.*, Realization of flat band with possible nontrivial topology in electronic Kagome lattice, Sci. Adv. **4**, eaau4511 (2018).

[29] M. Kang, S. Fang, L. Ye, H. C. Po, J. Denlinger, C. Jozwiak, A. Bostwick, E. Rotenberg, E. Kaxiras, J. G. Checkelsky *et al.*, Topological flat bands in frustrated kagome lattice CoSn, Nat. Commun. **11**, 4004 (2020).

[30] E. Tang, J.-W. Mei, and X.-G. Wen, High-Temperature Fractional Quantum Hall States, Phys. Rev. Lett. **106**, 236802 (2011).

[31] K. Sun, Z. Gu, H. Katsura, and S. Das Sarma, Nearly Flatbands with Nontrivial Topology, Phys. Rev. Lett. **106**, 236803 (2011).

[32] T. Neupert, L. Santos, C. Chamon, and C. Mudry, Fractional Quantum Hall States at Zero Magnetic Field, Phys. Rev. Lett. **106**, 236804 (2011).

[33] Z. Song, Z. Wang, W. Shi, G. Li, C. Fang, and B.A. Bernevig, All Magic Angles in Twisted Bilayer Graphene are Topological, Phys. Rev. Lett. **123**, 036401 (2019).

[34] Hoi Chun Po, L. Zou, T. Senthil, and A. Vishwanath, Faithful tight-binding models and fragile topology of magic-angle bilayer graphene, Phys. Rev. B **99**, 195455 (2019).

[35] J. Ahn, S. Park, and B.-J. Yang, Failure of Nielsen-Ninomiya Theorem and Fragile Topology in Two-Dimensional Systems with Space-Time Inversion Symmetry: Application to Twisted Bilayer Graphene at Magic Angle, Phys. Rev. X **9**, 021013 (2019).

[36] D. L. Bergman, C. Wu, and L. Balents, Band touching from real-space topology in frustrated hopping models, Phys. Rev. B **78**, 125104 (2008).

[37] D.-S. Ma, Y. Xu, C. S. Chiu, N. Regnault, A. A. Houck, Z. Song, and B. A. Bernevig, Spin-Orbit-Induced Topological Flat Bands in Line and Split Graphs of Bipartite Lattices, Phys. Rev. Lett. **125**, 266403 (2020).

[38] J.-W. Rhim and B.-J. Yang, Classification of flat bands according to the band-crossing singularity of Bloch wave functions, Phys. Rev. B **99**, 045107 (2019).

[39] J.-W. Rhim and B.-J. Yang, Singular flat bands, Adv. Phys.: X **6**, 1901606 (2021).

[40] J.-W. Rhim, K. Kim, and B.-J. Yang, Quantum distance and anomalous Landau levels of flat bands, Nature (London) **584**, 59 (2020).

[41] Y. Hwang, J. Jung, J.-W. Rhim, and B.-J. Yang, Wave-function geometry of band crossing points in two dimensions, Phys. Rev. B **103**, L241102 (2021).

[42] B. Sutherland, Localization of electronic wave functions due to local topology, Phys. Rev. B **34**, 5208 (1986).

[43] J. Vidal, R. Mosseri, and B. Douçot, Aharonov-Bohm Cages in Two-Dimensional Structures, Phys. Rev. Lett. **81**, 5888 (1998).

[44] J. Vidal, P. Butaud, B. Douçot, and R. Mosseri, Disorder and interactions in Aharonov-Bohm cages, Phys. Rev. B **64**, 155306 (2001).

[45] S. Mukherjee, A. Spracklen, D. Choudhury, N. Goldman, P. Öhberg, E. Andersson, and R. R. Thomson, Observation of a Localized Flat-Band State in a Photonic Lieb Lattice, Phys. Rev. Lett. **114**, 245504 (2015).

[46] N. Read, Compactly supported Wannier functions and algebraic *K*-theory, Phys. Rev. B **95**, 115309 (2017).

[47] W. Maimaiti, A. Andreanov, H. C. Park, O. Gendelman, and S. Flach, Compact localized states and flat-band generators in one dimension, Phys. Rev. B **95**, 115135 (2017).

[48] W. Maimaiti, S. Flach, and A. Andreanov, Universal $d = 1$ flat band generator from compact localized states, Phys. Rev. B **99**, 125129 (2019).

[49] M. Röntgen, C. V. Morfonios, and P. Schmelcher, Compact localized states and flat bands from local symmetry partitioning, Phys. Rev. B **97**, 035161 (2018).

[50] J. Ma, J.-W. Rhim, L. Tang, S. Xia, H. Wang, X. Zheng, S. Xia, D. Song, Yi Hu, Y. Li, B.-J. Yang, D. Leykam, and Z. Chen, Direct Observation of Flatband Loop States Arising from Nontrivial Real-Space Topology, Phys. Rev. Lett. **124**, 183901 (2020).

[51] A. Mielke, Ferromagnetic ground states for the Hubbard model on line graphs, J. Phys. A: Math. Gen. **24**, L73 (1991).

[52] A. Mielke, Ferromagnetism in the Hubbard model on line graphs and further considerations, J. Phys. A: Math. Gen. **24**, 3311 (1991).

[53] A. Mielke and H. Tasaki, Ferromagnetism in the Hubbard model, Commun. Math. Phys. **158**, 341 (1993).

[54] A. J. Kollár, M. Fitzpatrick, P. Sarnak, and A. A. Houck, Line-graph lattices: Euclidean and non-Euclidean flat bands, and implementations in circuit quantum electrodynamics, Commun. Math. Phys. **376**, 1909 (2020).

[55] Fa Wang and Y. Ran, Nearly flat band with Chern number $C = 2$ on the dice lattice, Phys. Rev. B **84**, 241103(R) (2011).

[56] M. Trescher and E. J. Bergholtz, Flat bands with higher Chern number in pyrochlore slabs, Phys. Rev. B **86**, 241111(R) (2012).

[57] S. Yang, Z.-C. Gu, K. Sun, and S. Das Sarma, Topological flat band models with arbitrary Chern numbers, Phys. Rev. B **86**, 241112(R) (2012).

[58] E. Kalesaki, C. Delerue, C. Morais Smith, W. Beugeling, G. Allan, and D. Vanmaekelbergh, Dirac Cones, Topological Edge States, and Nontrivial Flat Bands in Two-Dimensional Semiconductors with a Honeycomb Nanogeometry, Phys. Rev. X **4**, 011010 (2014).

[59] B. Pal, Nontrivial topological flat bands in a diamond-octagon lattice geometry, Phys. Rev. B **98**, 245116 (2018).

[60] A. Bhattacharya and B. Pal, Flat bands and nontrivial topological properties in an extended Lieb lattice, Phys. Rev. B **100**, 235145 (2019).

[61] See Supplemental Material at http://link.aps.org/supplemental/10.1103/PhysRevB.104.L081104 for more details about the definition and properties of CLS and FT-CLS, the relation between band crossing points of flat band and singular points of FT-CLS, the symmetry representation of flat band and SR-enforced band crossing. The detailed description of flat-band models is also included, which includes Refs. [68–92].

[62] C. Fang, M. J. Gilbert, and B. A. Bernevig, Bulk topological invariants in noninteracting point group symmetric insulators, Phys. Rev. B **86**, 115112 (2012).

[63] W. Beugeling, J. C. Everts, and C. Morais Smith, Topological phase transitions driven by next-nearest-neighbor hopping in two-dimensional lattices, Phys. Rev. B **86**, 195129 (2012).

[64] L. Zhang, J. Ren, J.-S. Wang, and B. Li, Topological magnon insulator in insulating ferromagnet, Phys. Rev. B **87**, 144101 (2013).

[65] A. Mook, J. Henk, and I. Mertig, Magnon Hall effect and topology in kagome lattices: A theoretical investigation, Phys. Rev. B **89**, 134409 (2014).

[66] R. Chisnell, J. S. Helton, D. E. Freedman, D. K. Singh, R. I. Bewley, D. G. Nocera, and Y. S. Lee, Topological Magnon Bands in a Kagome Lattice Ferromagnet, Phys. Rev. Lett. **115**, 147201 (2015).

[67] H. Yang, H. Nakano, and H. Katsura, Symmetry-protected topological phases in spinful bosons with a flat band, Phys. Rev. Research **3**, 023210 (2021).

[68] K. Shiozaki, M. Sato, and K. Gomi, Topological crystalline materials: General formulation, module structure, and wallpaper groups, Phys. Rev. B **95**, 235425 (2017).

[69] D. S. Dummit and R. M. Foote, *Abstract Algebra* (Wiley, Hoboken, NJ, 2004), Vol. 3.

[70] J. Zak, Symmetry Specification of Bands in Solids, Phys. Rev. Lett. **45**, 1025 (1980).

[71] J. Zak, Band representations and symmetry types of bands in solids, Phys. Rev. B **23**, 2824 (1981).

[72] B. Bradlyn, L. Elcoro, J. Cano, M. G. Vergniory, Z. Wang, C. Felser, M. I. Aroyo, and B. A. Bernevig, Topological quantum chemistry, Nature (London) **547**, 298 (2017).

[73] J. Cano, B. Bradlyn, Z. Wang, L. Elcoro, M. G. Vergniory, C. Felser, M. I. Aroyo, and B. A. Bernevig, Building blocks of topological quantum chemistry: Elementary band representations, Phys. Rev. B **97**, 035139 (2018).

[74] A. Alexandradinata and J. Höller, No-go theorem for topological insulators and high-throughput identification of Chern insulators, Phys. Rev. B **98**, 184305 (2018).

[75] J. Höller and A. Alexandradinata, Topological Bloch oscillations, Phys. Rev. B **98**, 024310 (2018).

[76] A. Alexandradinata, J. Höller, C. Wang, H. Cheng, and L. Lu, Crystallographic splitting theorem for band representations and fragile topological photonic crystals, Phys. Rev. B **102**, 115117 (2020).

[77] Li Chen, T. Mazaheri, A. Seidel, and X. Tang, The impossibility of exactly flat non-trivial Chern bands in strictly local periodic tight binding models, J. Phys. A: Math. Theor. **47**, 152001 (2014).

[78] L. Elcoro, B. J. Wieder, Z. Song, Y. Xu, B. Bradlyn, and B. A. Bernevig, Magnetic topological quantum chemistry, arXiv:2010.00598.

[79] Hoi Chun Po, H. Watanabe, and A. Vishwanath, Fragile Topology and Wannier Obstructions, Phys. Rev. Lett. **121**, 126402 (2018).

[80] J. Cano, B. Bradlyn, Z. Wang, L. Elcoro, M. G. Vergniory, C. Felser, M. I. Aroyo, and B.A. Bernevig, Topology of Disconnected Elementary Band Representations, Phys. Rev. Lett. **120**, 266401 (2018).

[81] B. Bradlyn, Z. Wang, J. Cano, and B.A. Bernevig, Disconnected elementary band representations, fragile topology, and Wilson loops as topological indices: An example on the triangular lattice, Phys. Rev. B **99**, 045140 (2019).

[82] A. Bouhon, A. M. Black-Schaffer, and R.-J. Slager, Wilson loop approach to fragile topology of split elementary band representations and topological crystalline insulators with time-reversal symmetry, Phys. Rev. B **100**, 195135 (2019).

[83] D. V. Else, Hoi Chun Po, and H. Watanabe, Fragile topological phases in interacting systems, Phys. Rev. B **99**, 125122 (2019).

[84] B. J. Wieder and B. A. Bernevig, The axion insulator as a pump of fragile topology, arXiv:1810.02373.

[85] S. Liu, A. Vishwanath, and E. Khalaf, Shift Insulators: Rotation-Protected Two-Dimensional Topological Crystalline Insulators, Phys. Rev. X **9**, 031003 (2019).

[86] Y. Hwang, J. Ahn, and B.-J. Yang, Fragile topology protected by inversion symmetry: Diagnosis, bulk-boundary correspondence, and Wilson loop, Phys. Rev. B **100**, 205126 (2019).

[87] A. Bouhon, T. Bzdušek, and R.-J. Slager, Geometric approach to fragile topology beyond symmetry indicators, Phys. Rev. B **102**, 115135 (2020).

[88] Zhi-Da Song, L. Elcoro, Y.-F. Xu, N. Regnault, and B.A. Bernevig, Fragile Phases as Affine Monoids: Classification and Material Examples, Phys. Rev. X **10**, 031001 (2020).

[89] Zhi-Da Song, L. Elcoro, and B. A. Bernevig, Twisted bulk-boundary correspondence of fragile topology, Science **367**, 794 (2020).

[90] V. Peri, Zhi-Da Song, M. Serra-Garcia, P. Engeler, R. Queiroz, X. Huang, W. Deng, Z. Liu, B. A. Bernevig, and S. D. Huber, Experimental characterization of fragile topology in an acoustic metamaterial, Science **367**, 797 (2020).

[91] R.-X. Zhang and Z.-C. Yang, Tunable fragile topology in floquet systems, Phys. Rev. B **103**, L121115 (2021).

[92] C. Weeks and M. Franz, Topological insulators on the Lieb and perovskite lattices, Phys. Rev. B **82**, 085310 (2010).